Applied Surface Science 493 (2019) 1243–1254

Contents lists available at ScienceDirect

Applied Surface Science

journal homepage: www.elsevier.com/locate/apsusc

Full length article

Compatibility of fabrication of superhydrophobic surfaces and addition of inhibitors in designing corrosion prevention strategies for electrodeposited nickel in saline solutions

Amir Hossein Noorbakhsh Nezhad[a], Reza Arefinia[b], Mehrdad Kashefi[a], Ali Davoodi[a,*], Saman Hosseinpour[c,*]

[a] Materials and Metallurgical Engineering Department, Faculty of Engineering, Ferdowsi University of Mashhad (FUM), Mashhad, Iran
[b] Chemical Engineering Department, Faculty of Engineering, Ferdowsi University of Mashhad (FUM), Mashhad, Iran
[c] Institute of Particle Technology (LFG), Friedrich-Alexander-Universität-Erlangen-Nürnberg (FAU), Cauerstrasse 4, 91058 Erlangen, Germany

ARTICLE INFO

Keywords:
Superhydrophobicity
Inhibitor
4-Mercaptopyridine
Nickel
Corrosion
Contact angle

ABSTRACT

The aim of this study is to assess the synergistic effect of two corrosion control strategies: application of an inhibitor and enhancing the surface superhydrophobicity, for protection of electrodeposited nickel in saline solutions. For this purpose, 4-Mercaptopyridine (C_5H_5NS) was added to the synthetic sea water solution and its corrosion inhibition efficiency was evaluated on electrodeposited smooth bright nickel layer and nickel films with hierarchical micro/nano structure. Stearic acid was used to tune the wetting properties of nickel films, from hydrophilic to superhydrophobic. Contact angle measurement, scanning electron microscopy, and Fourier-transform infrared spectroscopy were utilized in the characterization of deposited nickel layers. Potentiodynamic polarization and electrochemical impedance spectroscopy were employed to assess the corrosion inhibition performance of inhibitor on different nickel films. Our results indicate that simultaneous increase in the surface hydrophobicity and adsorption of corrosion inhibitor strategies does not yield a better corrosion resistance and that the most effective corrosion inhibition can be obtained on the bright smooth sample after a prolonged immersion in the corrosive solution. Furthermore, we show that the contact angle alone cannot be used to indicate the corrosion inhibition capability of an inhibitor.

1. Introduction

Superhydrophobic surfaces can offer anti-corrosion [1,2], anti-icing [3,4], antifouling [5,6], self-cleaning [7], and anti-bacterial [8] and superior tribological [9] properties and therefore are found in a wide range of applications such as medical devices, kitchen wares, buildings, maritime transport as well as automotive and aircraft industries. Liquid-infused slippery surfaces are also used in practical applications with promising repellant properties [9,10]. A superhydrophobic surface is defined as a surface with the water contact angle larger than 150°, and sliding angle lower than 10° [11,12]. Inspired by nature [13], multiple methods have been developed to artificially produce a superhydrophobic surface [14,15]. For instance, a rapid one-step procedure was developed by Chen et al. to fabricate superhydrophobic surfaces with hierarchical macro/nano scale cauliflower-like structure in an electrolytic cell containing myristic acid [16]. The same fatty acid was also recently used for fabrication of superhydrophobic nickel film on copper [17]. Li et al. prepared superhydrophobic ZnO surface by a simple combination of hydrothermal process and self-assemble monolayer deposition [18] whereas Latthe et al. fabricated transparent and thermally stable superhydrophobic silica films by the sol-gel co-precursor method [19]. Other methods such as plasma and chemical etching [20,21], layer-by-layer assembling [22,23], electrodeposition [24–26], chemical vapor deposition [27], as well as hybrid laser ablation/chemical modification [28] have also been used in the preparation of superhydrophobic surfaces. The shared feature among these methods is the combination of hierarchical micro/nano structures and the application of a low surface free energy material, in one or multiple fabrication steps [15]. Among these methods, electrodeposition is one of the most favored ones due to its low-cost of manufacturing, the ease in controlling the fabrication parameters, and the possibility of depositing a variety of simple layers and complex multilayers [29]. Electrodeposited coatings with different wetting properties may be applied in various electrodeposition baths by controlling critical parameters such

* Corresponding authors.
E-mail addresses: a.davodi@um.ac.ir (A. Davoodi), saman.hosseinpour@fau.de (S. Hosseinpour).

https://doi.org/10.1016/j.apsusc.2019.07.088
Received 15 May 2019; Received in revised form 2 July 2019; Accepted 12 July 2019
Available online 16 July 2019
0169-4332/

as temperature, applied current, pH, ion concentration, deposition time, and the presence of co-adsorbates [30–35].

Electrodeposition of nickel (Ni) on steel, often with an intermediate copper (Cu) layer, using non-toxic chemicals is considered as an effective and environmental friendly method to improve the corrosion resistance of the substrate. Adsorption of stearic acid (SA) on metallic surfaces via self-assembly also provides a noticeable corrosion protection to the substrate [36,37]. Thus, in industrial applications (SA) can be used, as a low surface free energy material, to chemically modify the roughened surface of electrodeposited Ni and to make it superhydrophobic with improved corrosion resistance properties [38–42].

Another common strategy in improving the corrosion resistance and reducing the corrosion rate of metals is the application of corrosion inhibitors, often in small amounts in ppm level [43,44]. Formation of complexes between inhibitors and metal surfaces is the main mechanism in which an inhibitor protects a surface from corrosion. Inhibitor/metal interaction depends upon the structure of inhibitor, electronic structure of inhibitor and substrate, hydrodynamic flow condition, as well as the adsorption competition between the inhibitor and other solution constituents [45]. For instance, pyridine derivatives are observed to improve the corrosion resistance of mild steel in HCl containing solution [46], especially under stagnant condition [47].

Despite the fact that the above-mentioned strategies, i.e. application of inhibitors and improving surface hydrophobicity, have been successfully utilized separately to improve the corrosion performance of metallic substrates, however, their synergistic effect via simultaneous application of these two strategies has not yet been studied. In this paper, we address the collegial effect of formation of a superhydrophobic surface and addition of an inhibitor, 4-mercaptopyridine (4Mpy, C_5H_5NS), on corrosion behavior of Ni films in 3.5 wt% NaCl solution. For this purpose, we first deposited Ni films with different surface structure and wettability and thoroughly characterized their microstructural and surface chemistry using scanning electron microscopy equipped with energy dispersive spectroscopy (SEM/EDS), contact angle (CA) measurement, and Fourier-transform infrared (FTIR) spectroscopy. Then we assessed the corrosion behavior of as-deposited Ni film (hereafter, bright film), structured Ni film (hereafter, hydrophilic film), and the structured Ni film with adsorbed SA layer (hereafter, superhydrophobic film), with and without the presence of the inhibitor in solution, with electrochemical measurements such as electrochemical impedance spectroscopy (EIS) and potentiodynamic polarization (PDP).

2. Experimental

2.1. Preparation of bright Ni coating

A bright film was prepared by electrodeposition of Ni layer on a Cu support. For this purpose, a pure Cu disc with a thickness of 1 mm and diameter of 1 cm, which was mounted in a polymeric resin, was used as the cathode. The cathode was ground and polished using successive grades of SiC paper (down to 3000 grade) and alumina slurry on polishing cloth. Then, the sample was electropolished at 20 $mA{\cdot}cm^{-2}$ for 1 min in a solution comprising 50 $g{\cdot}L^{-1}$ disodium carbonate (Na_2CO_3) and 10 $g{\cdot}L^{-1}$ potassium hydroxide (KOH). Finally, the sample was put in 10 wt% hydrochloric acid (HCl) solution at 25 °C for 30 s and washed by deionized water.

A 99.5% nickel (Ni) sheet (40 mm × 40 mm × 1 mm) was used as the anode. Both cathode and anode were immersed in an electrodeposition bath containing 240 $g{\cdot}L^{-1}$ nickel sulfate hexahydrate ($NiSO_4{\cdot}6H_2O$), 75 $g{\cdot}L^{-1}$ nickel chloride hexahydrate ($NiCl_2{\cdot}6H_2O$), 45 $g{\cdot}L^{-1}$ boric acid (H_3BO_3), and a commercial brightener agent. The electrodeposition bath was stirred with a magnetic stirrer and its temperature was kept at 60 ± 1 °C. The current density was set at 20 $mA{\cdot}cm^{-2}$ for 8 min to deposit a bright Ni layer with a thickness of ~3.5 μm.

2.2. Preparation of hydrophilic and superhydrophobic Ni coatings

Hydrophilic and superhydrophobic Ni coatings were also electrodeposited on a Cu support. The cathode and anode were prepared similar to the previous section while the bath contained 200 $g{\cdot}L^{-1}$ nickel chloride hexahydrate ($NiCl_2{\cdot}6H_2O$), 30 $g{\cdot}L^{-1}$ ammonium chloride (NH_4Cl), and 150 $g{\cdot}L^{-1}$ boric acid (H_3BO_3). The electrodeposition bath was similarly stirred with a magnetic stirrer and its temperature was kept at 60 ± 1 °C. To fabricate a Ni film with micro/nano hierarchical structure, two current density levels were applied using a DC power supply. First, the current density was set to 20 $mA{\cdot}cm^{-2}$ for 8 min. Then, the current density was adjusted to 50 $mA{\cdot}cm^{-2}$ for 1 min. The fabricated hydrophilic surface was then chemically modified with 6 $mmol{\cdot}L^{-1}$ stearic acid in ethyl alcohol for 10 min to achieve a superhydrophobic surface.

2.3. Surface characterization

The surface morphology of the electrodeposited films was assessed with an SEM/EDS (Leo 1450 VP/equipped with EDS Oxford instruments X-Max, England). Surface chemical composition was analyzed by a FTIR (Thermo Nicolet-AVATAR 370) with 4 cm^{-1} resolution and 32 scans. The CA measurements were performed with 4 μL water droplet at ambient temperature, using an optical contact angle meter (Adeeco static/dynamic). The ImageJ software was used to analyze the CA results.

2.4. Electrochemical measurements

All electrochemical measurements were performed in 3.5 wt% NaCl containing aqueous solutions with and without 4Mpy, at room temperature using an Autolab potentiostat/galvanostat instrument (PGSTAT 302 N). Following our previous study [47], we used 0.2 $g{\cdot}L^{-1}$ of 4Mpy in this work, as in the case of similar inhibitor (i.e. 2-mercaptopyridine) 0.2 $g{\cdot}L^{-1}$ concentration of inhibitor provided an optimum corrosion protection efficiency on steel with the efficiency of > 98%. Saturated calomel electrode (SCE) and platinum plate were used as reference and counter electrodes, respectively. The reference electrode was set in the nearest possible distance from the working electrode. The samples were immersed in the solutions for at least 0.5 h to be stabilized prior to the PDP measurements. PDP curves were obtained at a scanning rate of 1 $mV{\cdot}s^{-1}$ ranging from −300 mV vs. open circuit potential (OCP) to potentials that gave the current density of 1 $mA{\cdot}cm^{-2}$. Similar PDP tests were repeated for samples after immersion in 3.5 wt% NaCl solution for 120 h. The EIS measurements were conducted in the frequency range between 0.01 Hz and 100 kHz, with a sinusoidal signal perturbation of ± 10 mV. EIS measurements for bright Ni, hydrophilic film, and superhydrophobic film were performed after different immersion times (30 min, 2 h, 4 h, 6 h, 8 h, 10 h, 24 h, 48 h, 120 h, 168 h, 216 h, 288 h) in 3.5 wt% NaCl solution. The experimental EIS spectra were interpreted based on the equivalent electrical circuit and the Zview software was used to obtain the electrochemical fitting parameters. Beside the choice of suitable equivalent circuit model with a relevant physical meaning, the accuracy of the EIS fitting parameters was guaranteed by maintaining the fitting errors below 5%.

3. Results and discussion

3.1. Surface morphology and chemistry of the electrodeposited Ni films

Fig. 1(a–c) shows the surface morphology of the electrodeposited micro/nano structured Ni film, in different magnifications. The microstructure of the electrodeposited micro/nano structured Ni film, prepared by two current density levels, is consistent with the previously reported structures on similar systems [38,48]. These figures clearly depict the formation of so-called micro/nano cone-shaped structures.

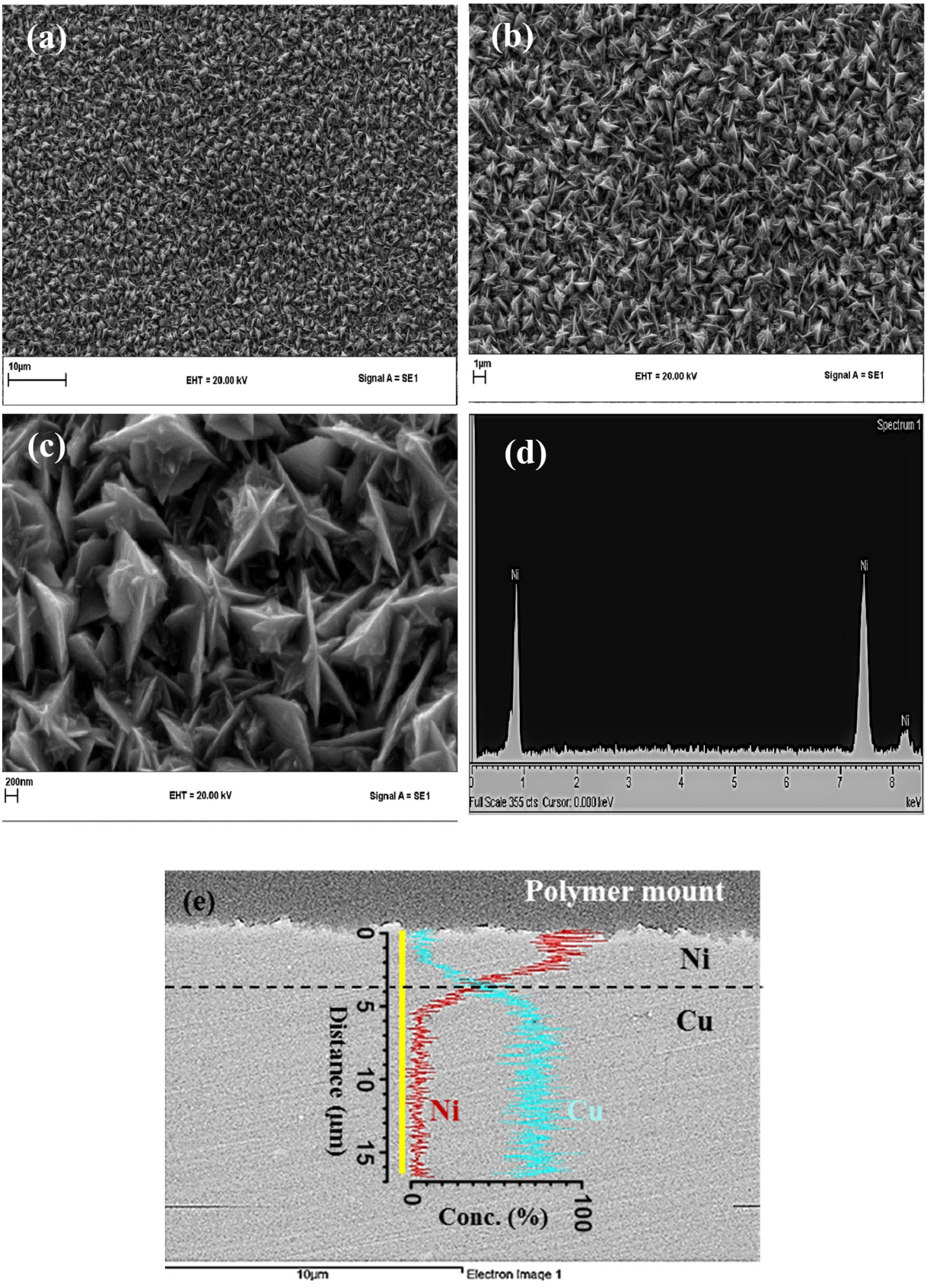

Fig. 1. (a–c) SEM surface morphology of the micro-nano structured Ni film on a Cu substrate with different magnifications. (d) EDS analyses of the micro-nano structured electrodeposited film (e) Cross-sectional SEM images. The inset shows the EDS elemental line profile analysis along the yellow line. The interface between Cu substrate and Ni film is marked with a dashed line based on the EDS line profile results.

Previous experimental and simulation studies showed that micro-nano cones form with a screw-dislocation driven crystal growth mechanism [49,50]. According to the classical crystal growth theory supersaturation of ionic species controls the driving force for crystal growth [51] and screw-dislocation driven growth is generally dominant at low supersaturation [52]. Therefore, in the first step of electrodeposition, i.e. in low current density level, preferential nickel ions growth on the screw-dislocations result in the formation of micro cones. Whereas in the second step of electrodeposition, i.e. when the high current density is applied, nickel ions may grow non-preferentially anywhere and therefore nano cones are formed.

Fig. 1d shows the EDS analysis of the freshly prepared micro-nano structured film right after electrodeposition. The EDS spectra taken from multiple points on the sample were consistent. The absence of Cu peak in the EDS results confirms the full coverage of the Cu substrate with the electrodeposited Ni film. In Fig. 1e the SEM cross-section of the micro-nano structured Ni film and the Cu substrate is presented where no contrast is observed between the Cu substrate and the Ni film. However, combined with the EDS line profile for Cu and Ni along the line marked with the yellow line the interface between the Cu substrate and the micro-nano structured Ni film is determined 4 µm from the surface and is marked with a dashed line.

Similarities between the FTIR spectra obtained from the superhydrophobic film and that of SA powder (Fig. 2) confirm that the adsorption of SA, as low surface free energy material, is responsible for the formation of the superhydrophobic surface. In these spectra, peaks at ~2918 cm^{-1} and ~2850 cm^{-1} correspond to asymmetric and symmetric CH_2 in SA, respectively. The peak at ~2940 cm^{-1} appears due to the Fermi resonance splitting of stretching and bending overtone of methyl group [53] in SA. The peaks at ~1700 cm^{-1} and ~1469 cm^{-1} are related to C=O and bending methylene vibrations $\delta(CH_2)$ in SA, respectively [54].

3.2. Wettability

Photographs of water droplets on samples with bright Ni, hydrophilic, and superhydrophobic coatings are shown in Fig. 3(a–c). Electrodeposited bright Ni film (Fig. 3a) shows a CA of 80°, which is consistent with previous works on similar films [24,25,55]. With the formation of micro/nano hierarchical structure the CA of Ni layer decreases dramatically and on the freshly prepared sample it approaches values below 10°. As described by Khorsand et al. [48] the reduction of CA upon the formation of micro/nano structure can be explained by Wenzel's model which assumes a full penetration of water into the troughs of the surface texture [56,57]. According to this model, increasing the surface roughness of hydrophilic surfaces with high surface free energy results in the reduction of CA to very low values. Adsorption of airborne organic hydrocarbons on the hydrophilic surface results in a gradual increase of CA [48] upon sample exposure to the lab air, therefore, the CA measurements on hydrophilic surfaces were performed on freshly electrodeposited films. Similarly, adsorption of SA, as a low surface free energy material, on the hierarchical nano/micro structures transforms the surface to a superhydrophobic surface with the CA > 150° (Fig. 3c). According to the Cassie-Baxter model [58] after treating the hierarchical micro/nano structures with SA, air pockets will be trapped underneath the liquid, which results in an increase of CA. Similar properties are obtained in slippery surfaces where the repellence performance relies on infused oil layer rather than air gap [9]. Based on this model the CA may be calculated by following equation [58]:

$$\cos\theta_{CB} = f_s((\cos\theta_0 + 1) - 1) \quad (1)$$

where θ_{CB} is the CA of the liquid droplet on the structured surface, θ_0 is the intrinsic CA on a flat surface, and f_s is the fraction of solid-liquid contact [58]. Fig. 3 (d–g) clearly shows that a drop of water does not stick to the superhydrophobic surface and is easily detached when the needle tip is retracted. However, the presence of the needle in these measurements might slightly interfere with the shape of droplets, rendering these results only valid for qualitative analysis.

3.3. Electrochemical measurements

In order to assess the collegial effect of surface hydrophobicity and addition of an organic inhibitor on the corrosion of Ni in saline solution, we performed electrochemical measurements (PDP and EIS) on samples with different degrees of hydrophobicity (i.e. hydrophilic, hydrophobic, and superhydrophobic) with and without the addition of 4Mpy as a corrosion inhibitor.

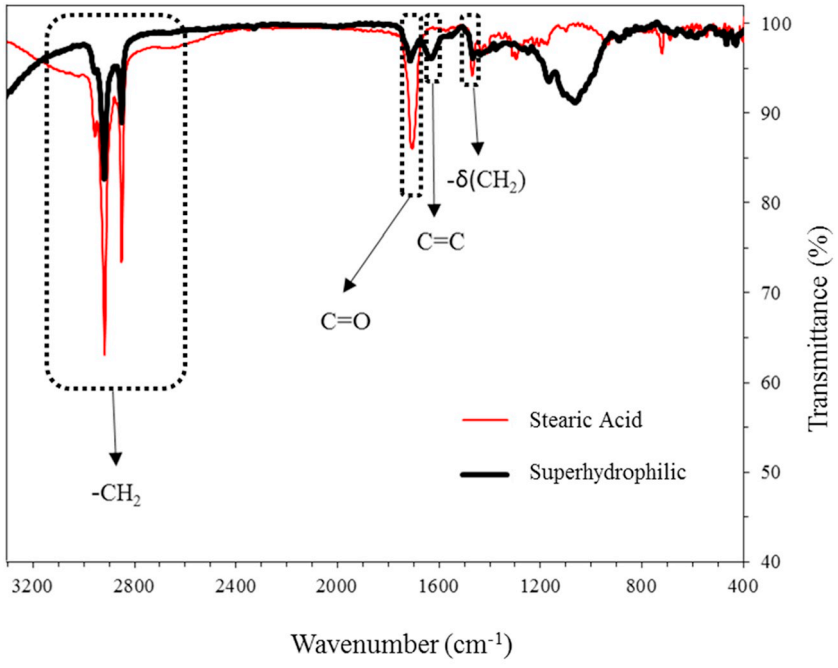

Fig. 2. FTIR spectra of superhydrophobic electrodeposited film and stearic acid powder. The resolution was set to 4 cm^{-1} and the number of scans was 32.

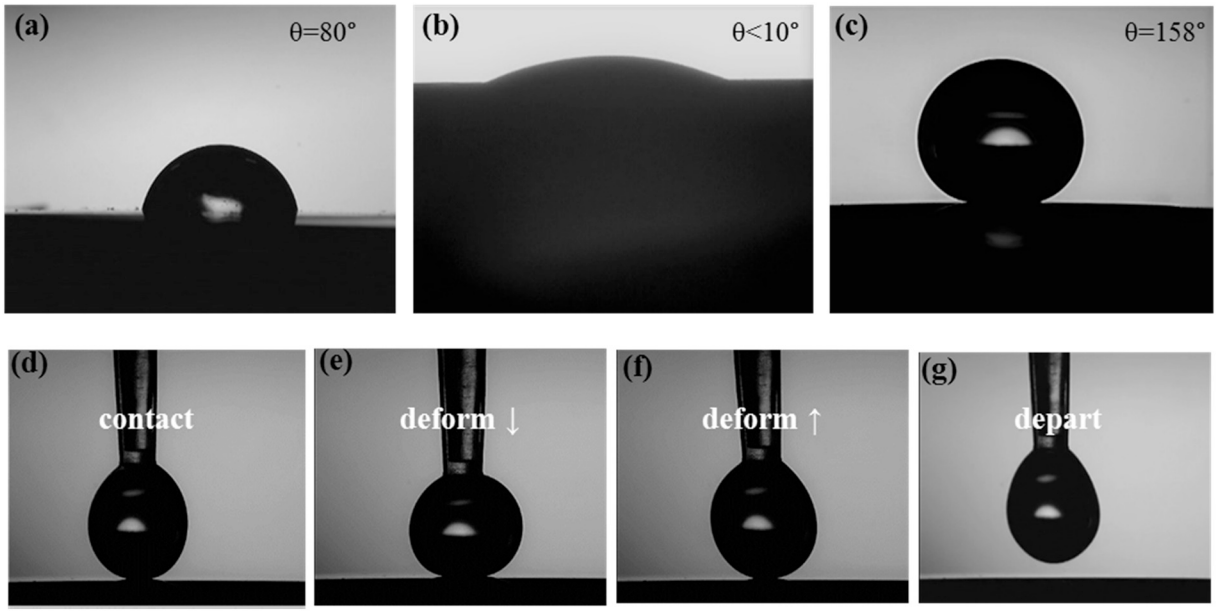

Fig. 3. Photographs of water droplets during the contact angle measurement on (a) bright Ni (b) hydrophilic and (c) superhydrophobic surfaces. (d–g) Steps showing the water droplet contacts the superhydrophobic surface, deforms during the approach, deforms during the departure, and finally departs the surface. The water droplet does not stick to the superhydrophobic surface and is easily detached.

3.3.1. Potentiodynamic polarization

The results from PDP measurements on electrodeposited bright Ni, hydrophilic Ni, and superhydrophobic Ni with and without 0.2 $g{\cdot}L^{-1}$ 4Mpy after 30 min immersion in 3.5 wt% NaCl solution are presented in Fig. 4a. To evaluate the effect of immersion time on the corrosion behavior of these samples, the corresponding PDP results after 120 h sample immersion in 3.5 wt% NaCl solution are provided in Fig. 4b. The corrosion current density (i_{corr}), corrosion potential (E_{corr}), the slope of the cathodic region (β_c), and the slope of the anodic region (β_a) are calculated using Tafel extrapolation method and reported in Table 1. Apparent surface area is used for all these calculations. In this table the corrosion inhibitor efficiency of inhibitor which is calculated via the following equation is also provided;

$$\%\eta = \frac{i^0_{corr} - i_{corr}}{i^0_{corr}} \times 100 \quad (2)$$

In this equation, i^0_{corr} and i_{corr} are corrosion current densities of each Ni film in the absence and presence of inhibitor, respectively [59].

As is evident from PDP results and results in Table 1, for short immersion times (Fig. 4a) corrosion rate of the bright electrodeposited Ni film is higher than that of the hydrophilic film, and superhydrophobic sample exhibits the lowest corrosion rate. Formation of an air layer in the micro-nano grooves of the superhydrophobic surface is responsible for the low i_{corr} and therefore low corrosion rate of the superhydrophobic surface [27,55]. This air layer forms between the sample surface and the electrolyte and limits the access of aggressive electrolyte and consequently the electron transfer in this region [25]. Addition of inhibitor to the system, improves the corrosion performance of all

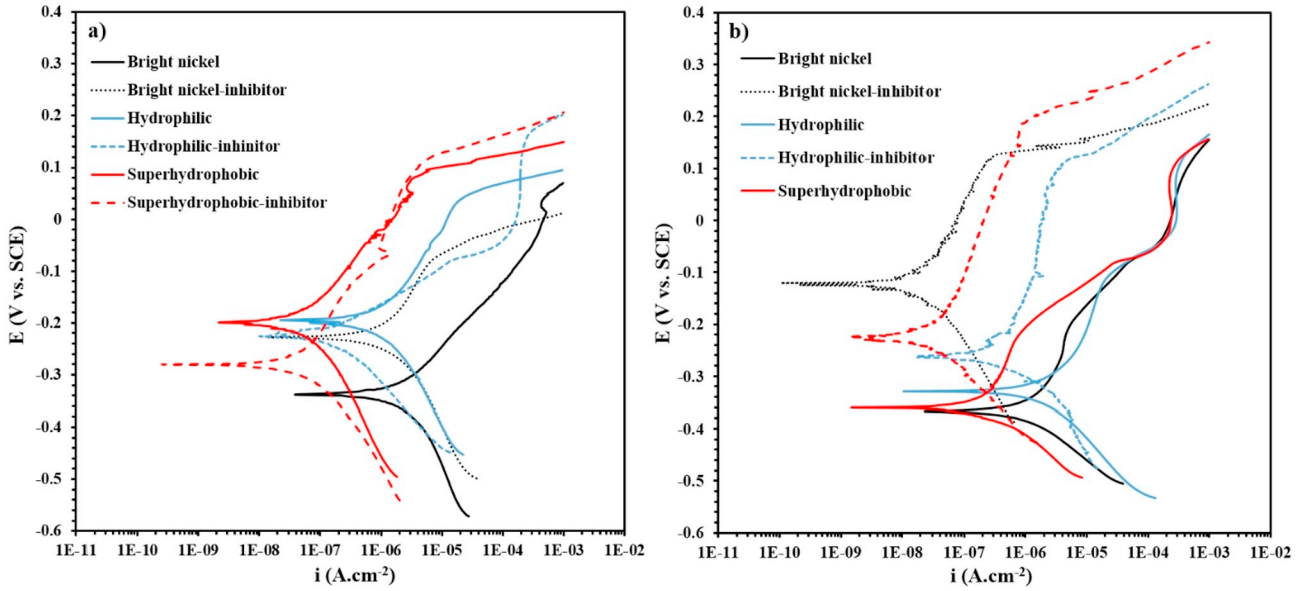

Fig. 4. The potentiodynamic polarization curves of bright, hydrophilic, and superhydrophobic electrodeposited Ni film in 3.5 wt% NaCl solutions with and without inhibitor (a) after 30 min (b) after 120 h immersion.

Table 1
Electrochemical parameters obtained from the polarization curves in the presence and absence of 4Mpy in 3.5 wt% NaCl solution after 30 min (after OCP stability immersion) and 120 h (long time immersion).

Sample	β_a (V/dec)	β_c (V/dec)	E_{corr} (V vs. SCE)	i_{corr} (A/cm^2)	%η
Bright nickel - 30 min	0.13	0.18	−0.34	2.07E−06	–
Bright nickel – inhibitor - 30 min	0.16	0.20	−0.22	1.21E−06	41.6
Bright nickel - 120 h	0.17	0.09	−0.37	1.01E−06	–
Bright nickel - inhibitor - 120 h	0.145	0.20	−0.12	1.85E−08	98.2
Superhydrophobic - 30 min	0.15	0.14	−0.20	4.88E−08	–
Superhydrophobic - Inhibitor - 30 min	0.13	0.17	−0.27	4.63E−08	5.2
Superhydrophobic - 120 h	0.10	0.27	−0.35	2.47E−07	–
Superhydrophobic - inhibitor - 120 h	0.21	0.12	−0.22	2.92E−08	88.1
Hydrophilic - 30 min	0.16	0.15	−0.20	8.55E−07	–
Hydrophilic -inhibitor - 30 min	0.32	0.09	−0.33	8.00E−07	6.5
Hydrophilic - 120 h	0.16	0.12	−0.33	1.98E−06	–
Hydrophilic -inhibitor - 120 h	0.11	0.51	−0.26	6.53E−07	67.1

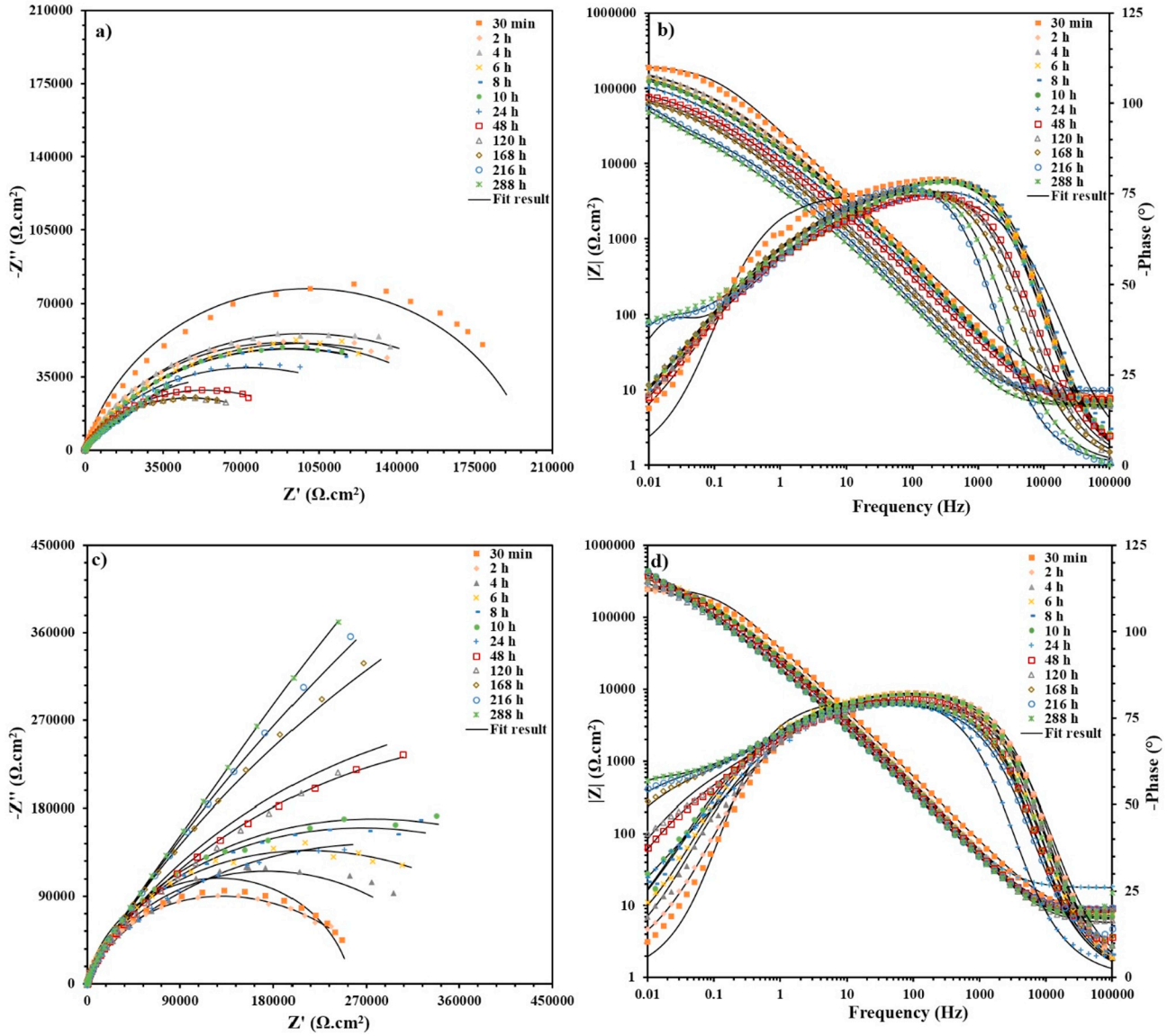

Fig. 5. EIS results for superhydrophobic Ni film without inhibitor (a) Nyquist and (b) Bode (resistance magnitude and phase angle) representation. (c) and (d) show the Nyquist and Bode results for the superhydrophobic sample with 0.2 g/L 4Mpy inhibitor in solution. EIS curves for different immersion times are presented with different symbols. Lines are fits to the experimental data (symbols).

samples and the order in corrosion rates remains as bright film > hydrophilic film > superhydrophobic film. However, the extent of which the corrosion performance is improved with the introduction of the inhibitor to the system is different on these samples. Addition of inhibitor provides an initial inhibition efficiency of > 40% to the bright Ni film, whereas its corrosion inhibition efficiency on the samples with

micro/nano structures is very low (i.e. ~6% and ~5% for hydrophilic and superhydrophobic samples, respectively). We hypothesize that energy barrier (i.e. surface repulsion force) for the adsorption of inhibitor on the samples with micro/nano structures is larger than that for the smooth film (i.e. bright sample). Presence of hydrophobic SA molecules on the superhydrophobic surfaces may also further prevent the adsorption of the inhibitor on this surface. After 120 h immersion in 3.5 wt% NaCl solution, i_{corr} decreased for the bright Ni film whereas it increases for samples with micro/nano structures (i.e. hydrophilic and superhydrophobic films). Surface oxide growth on the bright sample upon prolonged immersion is responsible for the reduction of i_{corr} on this sample. In contrast, for the samples with the micro/nano structures, especially on the hydrophilic sample with the lowest CA, the concentration of corrosive ions in the surface micro-nano grooves increases by time and thus leads to increase of i_{corr} on these samples. The order of i_{corr} on samples after 120 h immersion in 3.5 wt% NaCl becomes as; hydrophilic film > bright film > superhydrophobic film. As was discussed earlier, the addition of inhibitor to the solution reduces the corrosion rate of all samples. Presence of the inhibitor in solution for the samples with prolonged immersion time results in a higher corrosion inhibition efficiency compared to those with shorter immersion time and after 120 h immersion, the corrosion inhibition of inhibitor reaches > 98%, 88%, and 67% for bright, superhydrophobic, and hydrophilic electrodeposited Ni films, respectively.

As is evidenced by the PDP results, simultaneous implementation of the two common corrosion control strategies, i.e. fabrication of superhydrophobic surfaces and introduction of inhibitors, does not improve the corrosion resistance of electrodeposited Ni films in saline solutions. In fact, the best corrosion performance is obtained either by fabrication of a superhydrophobic surface without the addition of an inhibitor or by application of inhibitors on smooth surfaces.

3.3.2. Electrochemical impedance spectroscopy (EIS)

Multiple parameters such as surface microstructure, surface wettability, adsorption of inhibitors or other organic molecules to the surface, as well as surface oxide growth affect the interactions between the electrode (i.e. electrodeposited Ni film in this case) and the electrolyte (3.5 wt% NaCl solution). Indeed, such interactions may alter by time, as the electrode surface evolves. In order to gain a deeper understanding on the contribution of different parameters in the corrosion of electrodeposited Ni films in saline solutions, with and without the presence of the inhibitor, we performed complementary EIS measurements and the results are discussed here.

The EIS results obtained on the superhydrophobic Ni film in 3.5 wt % NaCl solution with and without the inhibitor are plotted in Fig. 5 with the Nyquist and Bode (impedance module and phase angle shift) representations. Similar measurements were performed on the hydrophilic and bright Ni film and the corresponding results are provided in Figs. 6 and 7, respectively. The Bode magnitude and phase angle plots for all samples after prolonged immersion depict the existence of two or more time constants.

To perform a quantitative comparison between the effect of different interfacial layer constituents (i.e. solution, surface roughness, oxide layer, and the presence and absence of SA and inhibitor), we fitted the EIS data using equivalent circuit models. The surface constituents for the electrodeposited bright, hydrophilic, and superhydrophobic Ni films with and without the inhibitor are different. Furthermore, the surface of samples undergoes dynamic changes upon immersion in solution. Therefore, different equivalent circuit models were used to fit the EIS results in Figs. 5–7. The equivalent circuit models superimposed on schematic representations of sample surface are presented in Fig. 8 and the corresponding obtained fitting parameters are provided in Tables S1–S6 in the Supplementary information. A summary of the conclusions of these results are provided here:

(1) Superhydrophobic surface: As mentioned before, in the initial stages of sample immersion, the presence of an air gap layer between the hierarchical micro/nano structures of the superhydrophobic Ni film and electrolyte improves the corrosion resistance of the superhydrophobic coatings. The contact between the electrolyte and the sample in this stage is limited (Fig. 8a) and the corresponding EIS response can be expressed with one time constant and a Randle-like equivalent circuit consisting of a series link between R_s (solution resistance) and a CPE_1 (constant phase element, as a non-ideal capacitor) which is connected in parallel to a R_2 (charge transfer resistance of the electrolyte double layer), refer to Table S1 in Supplementary information. For n = 1, CPE has a unit of capacitance (F). The parameters C (capacitance), and CPE factors (Q and n) in this table are calculated using Eqs. (3) and (4) [25,43], where Q has a unit of ($\Omega \cdot cm^{-2}S^{-n}$).

$$C = \frac{(Q \times R)^{\left(\frac{1}{n}\right)}}{R} \tag{3}$$

$$CPE = \frac{1}{Q(j\omega)^n} \tag{4}$$

In these equations Q is the CPE constant, which nominally equals to the pure capacitance of the system for n = 1; $j^2 = -1$, ω is the angular frequency (rad/s), and the value of n ranges between 0 and 1. Time dependence EIS results show that this situation is stable up to the first few hours of immersion. With longer immersion time, up to 168 h, the volume of the air layer between the electrolyte and Ni surface decreases facilitating the access of electrolyte to Ni surface (Fig. 8b). At this stage, two time constants can be observed in the EIS results (Fig. 5a and b) which are considered in the additional elements in the equivalent circuit model as CPE_2 (constant phase element for surface Ni layer) and R_3 (charge transfer resistance of surface Ni layer). At 216 h immersion time, the electrolyte eventually penetrates to the Ni layer and may even reach the Ni/Cu interface at some points. As showed in Fig. 8c, the equivalent circuit at such prolonged immersion contains a Warburg element (W_s) representing a diffusion element in a short range. W_s is defined as Eq. (5) where R_{Ws} is the short-range Warburg coefficient, $T_{Ws} = d^2/D$ (d is the effective diffusion thickness, and D is the effective diffusion coefficient of the ion species), and n_{Ws} ranges between 0 and 1. The corresponding fitting parameters are provided in Table S1.

$$W_s = \frac{R_{Ws}\tanh((j\omega T_{Ws})^{n_{Ws}})}{(j\omega T_{Ws})^{n_{Ws}}} \tag{5}$$

Comparing Fig. 6a and c, it becomes clear that in the absence of inhibitor the corrosion resistance decreases by increasing the immersion time whereas in the presence of the inhibitor this trend is the opposite. In other words, the durability of the superhydrophobic film increases by adding inhibitor to the electrolyte. The extracted EIS parameters for the superhydrophobic sample immersed in an electrolyte with the inhibitor are reported in Table S2.

(2) Hydrophilic surface: The main difference between the electrodeposited hydrophilic and superhydrophobic Ni films is the absence of low surface energy material in the former and therefore the lack of the air layer between electrolyte and sample surface. Consequently, the electrolyte can easily penetrate through the surface grooves of the hydrophilic surface with low CA [55]. According to Fig. 6a and b, in the absence of the inhibitor, the EIS results for the initial hours of immersion exhibit a complicated behavior, which is due to the formation of an incomplete interfacial layer between the electrolyte and the micro/nano structured Ni film. At this stage corrosive Cl^- ions may penetrate into the mico/nano hierarchical grooves. The corresponding equivalent circuit is presented in Fig. 8d and the fitting parameters are provided in Table S3. Between 24 h and 48 h immersion, the surface is saturated with the solution and micro-nano grooves are filled completely. Accordingly, the equivalent circuit changes to Fig. 8e. With the

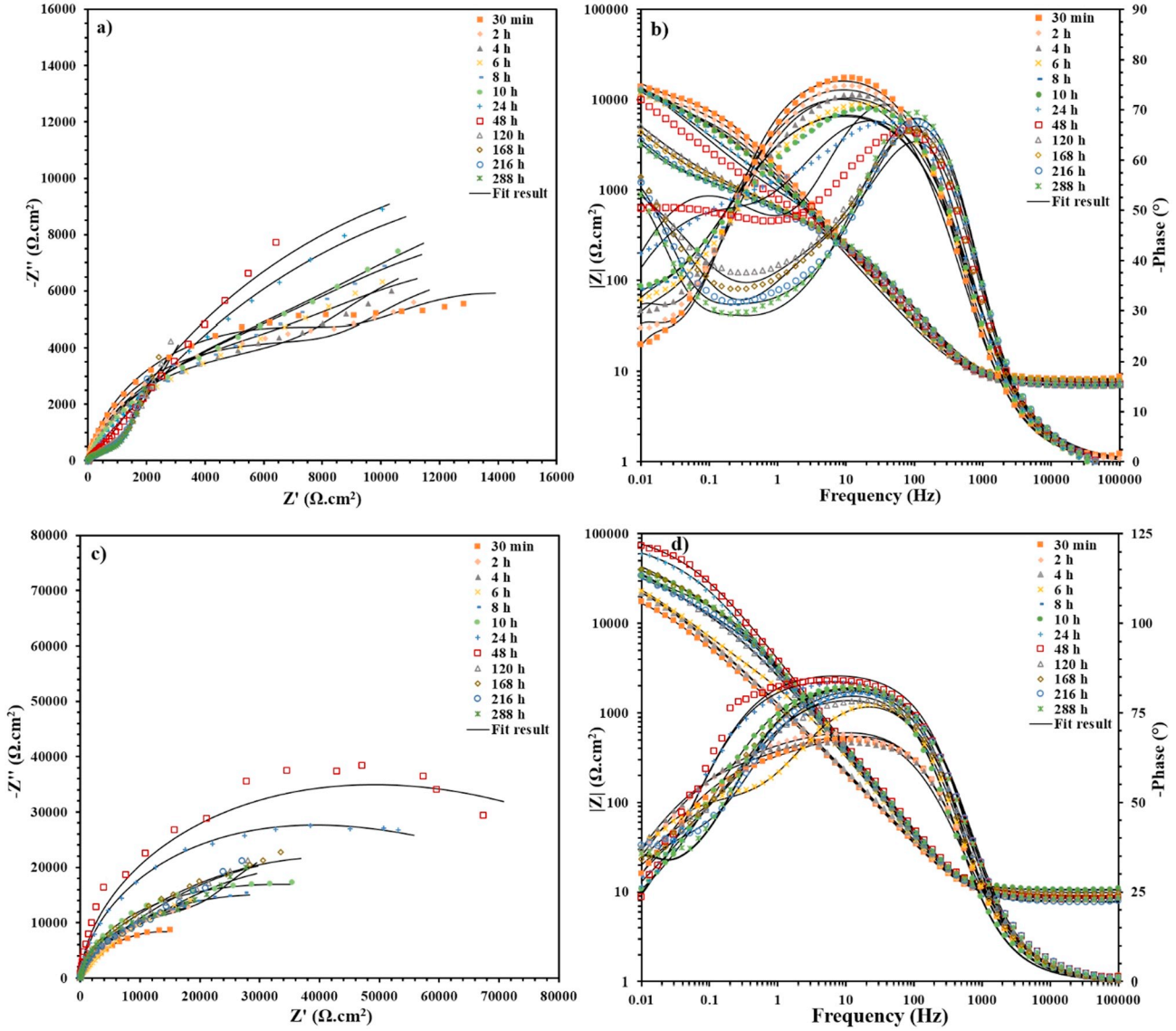

Fig. 6. EIS results for hydrophilic Ni film without inhibitor (a) Nyquist and (b) Bode (resistance magnitude and phase angle) representation. (c) and (d) show the Nyquist and Bode results for the superhydrophobic sample with 0.2 g/L 4Mpy inhibitor in solution. EIS curves for different immersion times are presented with different symbols. Lines are fits to the experimental data (symbols).

further immersion of the sample in solution, after 216 h, the solution may completely penetrate the Ni film and reach the Ni/Cu interface. The diffusion path at this stage becomes infinite and is not stable anymore. In this case, an infinite Warburg diffusion element (W_O) may be used in the equivalent circuit model (Fig. 8f) to describe the corresponding EIS results. The value of W_O is defined as:

$$W_O = \frac{R_{Wo}\coth((j\omega T_{Wo})^{nWo})}{(j\omega T_{Wo})^{nWo}} \quad (6)$$

where R_{Wo} is the long-range Warburg coefficient, $T_{Wo} = d^2/D$ (d is the effective diffusion thickness, and D is the effective diffusion coefficient of the ion species), and n_{Wo} ranges between 0 and 1. The corresponding fitting parameters are provided in Table S3.

When added to the solution, the corrosion inhibition property of 4Mpy results in a considerable reduction of the corrosion rate (Table S4), up to 120 h immersion (Fig. 6c and d), whereas the corrosion resistance of the system without inhibitor constantly declined in this period. After this initial period, corrosion resistance of the hydrophilic sample even in the presence of the inhibitor decreases and the corrosive electrolyte completely penetrates into the substrate.

(3) Bright Ni surface: Unlike the electrodeposited hydrophilic and superhydrophobic Ni films which feature hierarchical micro/nano structures, the bright Ni exposes a less complex surface structure to the electrolyte. Therefore, it is expected that the EIS response on this sample also differs from those on the micro/nano structured samples. Fig. 7a and b represent the EIS curves of the bright Ni sample for different immersion times in the absence of the inhibitor, where two time constants can be observed in all immersion times. The corresponding equivalent circuits as well as the fitting parameters are provided in Fig. 8 (g–i) and Table S5, respectively. According to these results, the corrosion resistance, and probably the thickness of the oxide layer, monotonically increases on this sample with prolonged immersion up to 48 h. Within the first 48 h immersion, the impedance (|Z|) rises from 18,800 Ω·cm^2 to 29,200 Ω·cm^2. After 48 h immersion, corrosion resistance declines due to the diffusion of electrolyte into the substrate.

According to Fig. 7c and d, EIS spectra of the bright Ni film reveal a

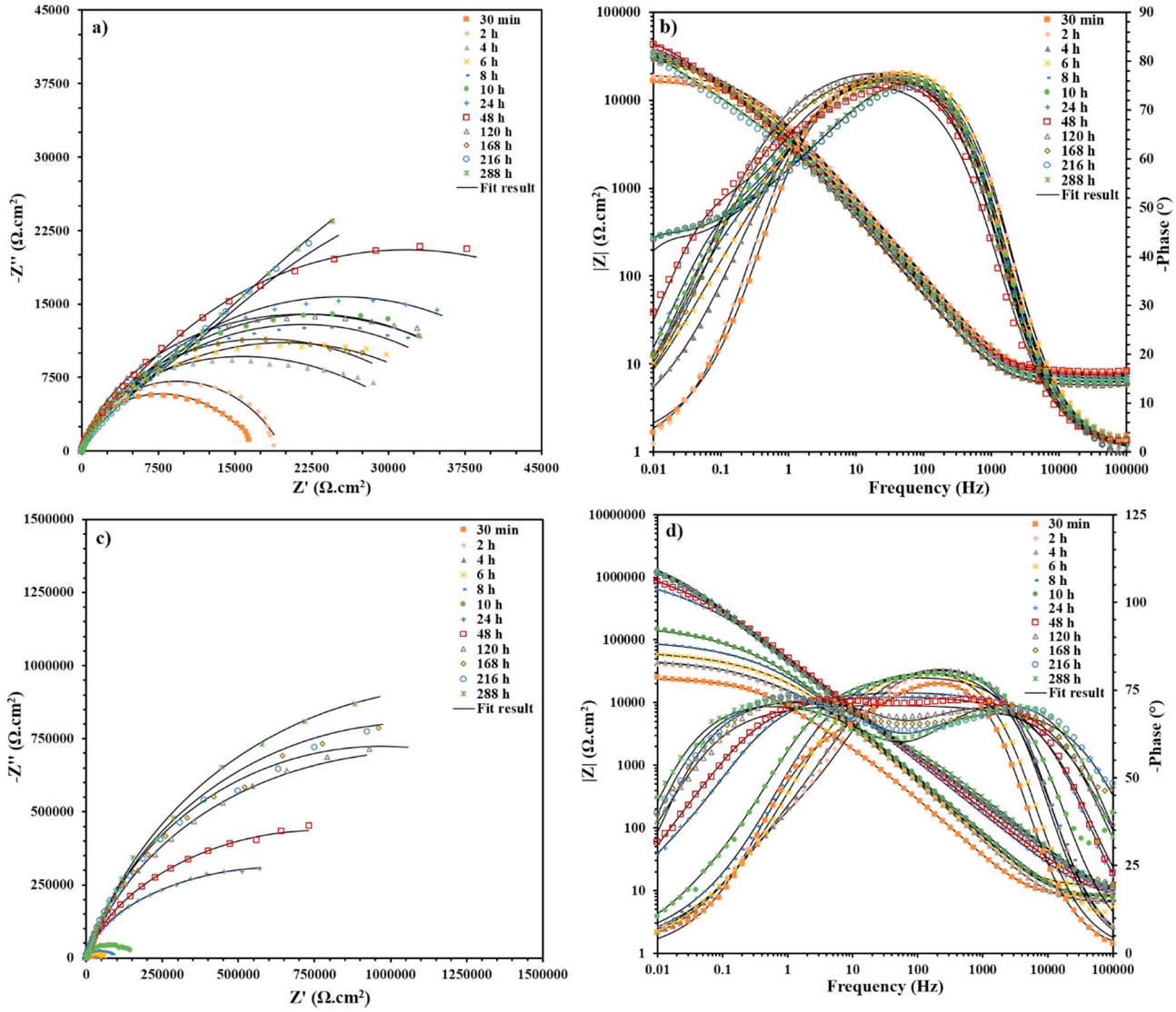

Fig. 7. EIS results for bright Ni film without inhibitor (a) Nyquist and (b) Bode (resistance magnitude and phase angle) representation. (c) and (d) show the Nyquist and Bode results for the superhydrophobic sample with 0.2 g/L 4Mpy inhibitor in solution. EIS curves for different immersion times are presented with different symbols. Lines are fits to the experimental data (symbols).

better corrosion performance of the sample in the presence of the inhibitor. The corresponding fitting parameters are presented in Table S6. Nevertheless, it is evident from this table that the corrosion inhibition efficiency of 4MPy reaches > 90% after 24 h immersion. The corrosion inhibition efficiency of the inhibitor on bright Ni film then decreases slightly up to 168 h immersion. Further prolongation of immersion (> 216 h) results in the penetration of electrolyte through the adsorbed inhibitor and causes instability of the protective layer. After this stage corrosion occurs in Ni film as well as on the Ni/Cu substrate. Fig. 9a and b graphically summarize the absolute impedance module (at 0.01 Hz) for different samples with and without the presence of the inhibitor and the corrosion inhibition efficiency of the inhibitor as a function of immersion time, respectively. The EIS results confirm that simultaneous application of corrosion control strategies (i.e. making the surface superhydrophobic and applying corrosion inhibitor) does not provide a beneficial synergistic effect, which is consistent with the conclusion from our PDP results (vide supra).

Along with the EIS measurements, the CA of water droplet over the superhydrophobic film with different immersion times in corrosive solution with and without the inhibitor was measured and the results are presented in Fig. 10. This figure demonstrates that by adding the inhibitor, the durability of superhydrophobicity increases as compared to that in solutions without inhibitor. In the presence of the inhibitor, the superhydrophobic film can maintain its superhydrophobic property during long time immersion (e.g. for > 120 h) in 3.5 wt% NaCl solution. Although the CA falls to values below 150° after 288 h immersion, this high CA indicates the good stability of the superhydrophobic property of the film in 3.5 wt% NaCl with 0.2 g/L 4Mpy solution whereas, without inhibitor in the solution, the CA reaches values close to 100 after 288 h immersion. It should be noted that after such relatively long immersion time (i.e. 288 h) in a solution containing the inhibitor, the electrodeposited superhydrophobic Ni film did not have the best corrosion performance (Fig. 9). Thus, it is clear that the measurement of water CA alone is not a sufficient criterion in designing corrosion control strategies and that time dependence PDP and EIS measurements can provide useful insights into the sustainability of the corrosion control strategy.

4. Conclusions

In this research, the corrosion inhibition efficiency of 4-mercaptopyridine (4Mpy) as an inhibitor on the electrodeposited smooth bright,

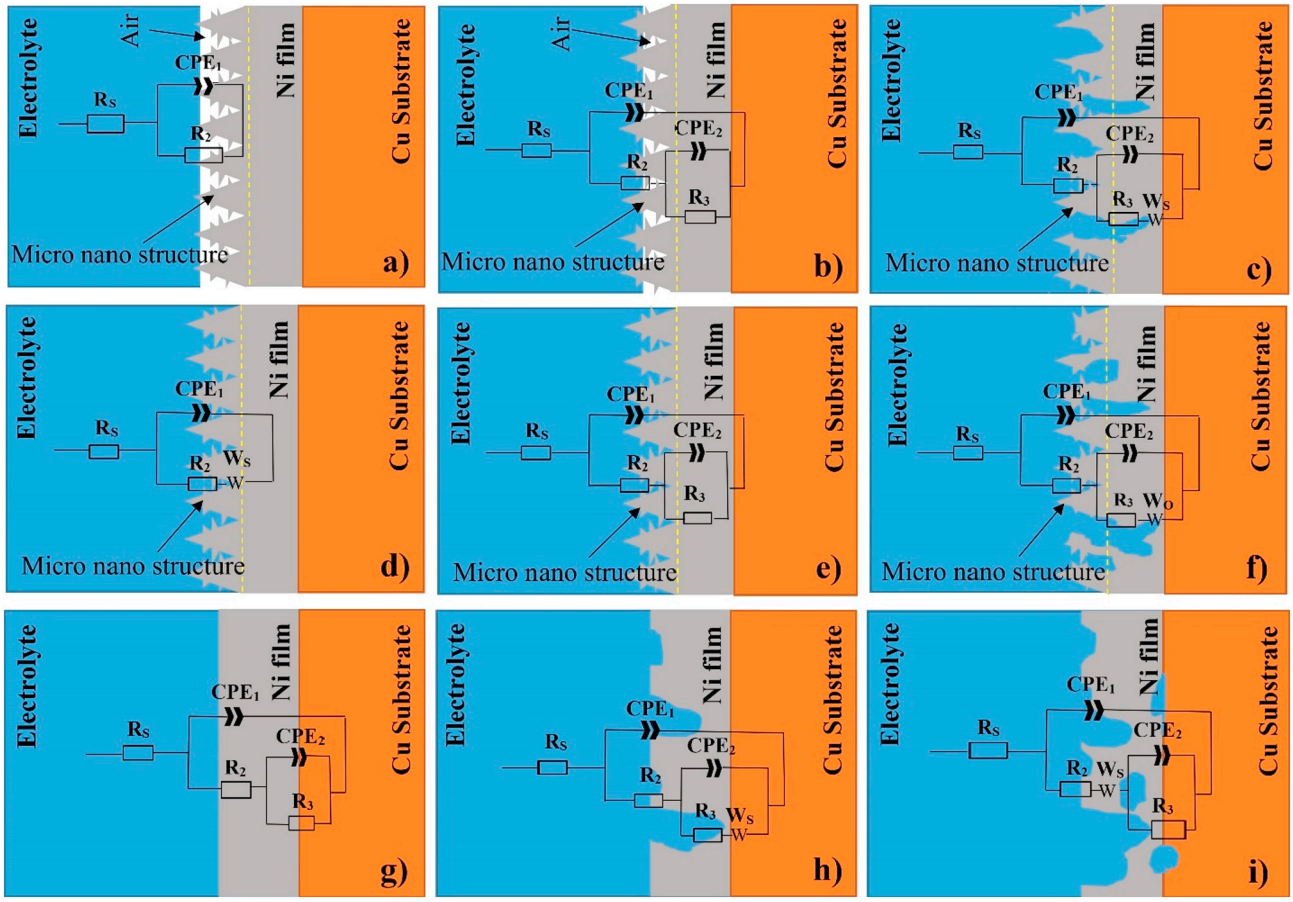

Fig. 8. Equivalent circuits models superimposed on the schematic representations of (a–c) superhydrophobic, (d–f) hydrophobic, and (g–i) bright Ni surface in solution. In (a–f) the micro and nano structures are schematically presented out of scale. The presence of the inhibitor in solution is not graphically shown here but is concluded in the corresponding equivalent circuit models. The equivalent circuit models in the left column correspond to the surface of samples in the initial stages of immersion. The middle and right columns represent changes of the surface constituents with prolonged immersion in corrosive solution. The obtained fitting parameters are presented in Tables in the Supplementary information.

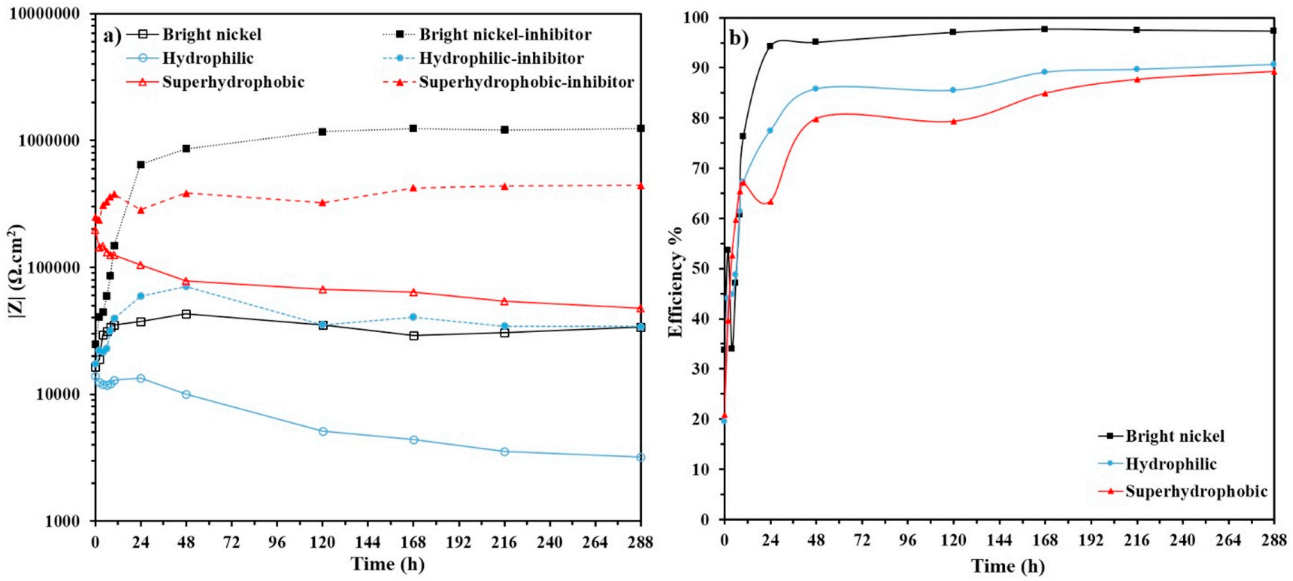

Fig. 9. Effect of immersion time on (a) absolute impedance module at 0.01 Hz and (b) corrosion inhibitor efficiency on bright, hydrophilic and superhydrophobic Ni surfaces immersed in 3.5 wt% NaCl solution. The lines connecting the symbols (experimental data) are guide to the eyes.

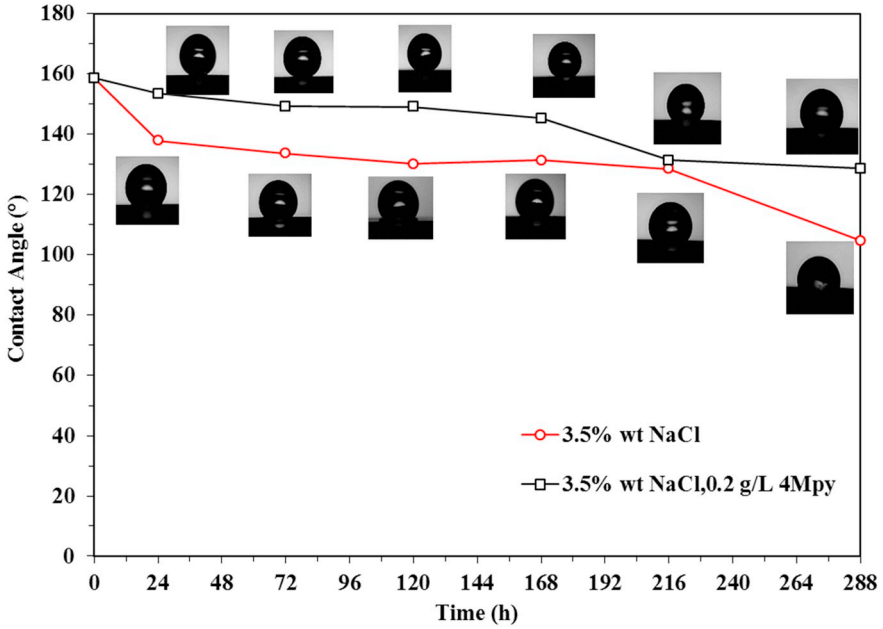

Fig. 10. Changes of water CA of the superhydrophobic surface with the immersion time in 3.5 wt% NaCl solution with and without 0.2 $g{\cdot}L^{-1}$ 4Mpy. The lines connecting the symbols (experimental data) are guide to the eyes.

hydrophilic, and superhydrophobic Ni films is investigated to address the question whether or not two common corrosion control strategies, i.e. fabrication of superhydrophobic surface and application of corrosion inhibitors, may exert beneficial synergistic effects. According to electrochemical measurements, despite the fact that the presence of inhibitor generally improved the corrosion performance of the Ni films, the most efficient inhibition effect of 4Mpy was observed on the bright Ni film after prolonged immersion in 3.5 wt% NaCl corrosive solution. The corrosion current density on the samples with inhibitor in solution were as; bright (18.5 $nA{\cdot}cm^{-2}$) < superhydrophobic (29.2 $nA{\cdot}cm^{-2}$) < hydrophilic (653 $nA{\cdot}cm^{-2}$). The bright Ni film also showed the highest polarization resistance, in compare with superhydrophobic and hydrophilic Ni film, after 5 days of immersion. This behavior may be related to the surface structure and low surface energy of the bright Ni film which accommodate adsorption of inhibitor molecules via electron donation. Our results show that simultaneous application of inhibitors and surfaces with high degrees of hydrophobicity (e.g. superhydrophobic surfaces) does not provide beneficial collegial effects. Finally, we showed that high CA values alone, even after long-time immersion, cannot be used as a reliable criterion in determining the corrosion inhibition capability of an inhibitor, and that complementary time dependence electrochemical measurements deem essential for designing the most efficient corrosion control strategies.

Acknowledgments

Ferdowsi University of Mashhad is appreciated for providing experimental setups. AHNN appreciates Ehsan Rahimi and Ali Rafsanjani-Abbasi for their valuable comments on the paper. SH thanks Emerging Talents Initiative (ETI) 2018/2_Tech_06, FAU, Germany grant for supporting his research.

Appendix A. Supplementary data

Supplementary data to this article can be found online at https://doi.org/10.1016/j.apsusc.2019.07.088.

References

[1] Z. She, Q. Li, Z. Wang, L. Li, F. Chen, J. Zhou, Researching the fabrication of anticorrosion superhydrophobic surface on magnesium alloy and its mechanical stability and durability, Chem. Eng. J. 228 (2013) 415–424.
[2] C.-J. Weng, C.-H. Chang, C.-W. Peng, S.-W. Chen, J.-M. Yeh, C.-L. Hsu, Y. Wei, Advanced anticorrosive coatings prepared from the mimicked xanthosoma sagittifolium-leaf-like electroactive epoxy with synergistic effects of superhydrophobicity and redox catalytic capability, Chem. Mater. 23 (2011) 2075–2083.
[3] S. Kulinich, M. Farzaneh, On ice-releasing properties of rough hydrophobic coatings, Cold Reg. Sci. Technol. 65 (2011) 60–64.
[4] Y. Wang, J. Xue, Q. Wang, Q. Chen, J. Ding, Verification of icephobic/anti-icing properties of a superhydrophobic surface, ACS Appl. Mater. Interfaces 5 (2013) 3370–3381.
[5] L. Zhao, Q. Liu, R. Gao, J. Wang, W. Yang, L. Liu, One-step method for the fabrication of superhydrophobic surface on magnesium alloy and its corrosion protection, antifouling performance, Corros. Sci. 80 (2014) 177–183.
[6] J.-S. Chung, B.G. Kim, S. Shim, S.-E. Kim, E.-H. Sohn, J. Yoon, J.-C. Lee, Silver-perfluorodecanethiolate complexes having superhydrophobic, antifouling, antibacterial properties, J. Colloid Interface Sci. 366 (2012) 64–69.
[7] X. Zhang, Y. Guo, Z. Zhang, P. Zhang, Self-cleaning superhydrophobic surface based on titanium dioxide nanowires combined with polydimethylsiloxane, Appl. Surf. Sci. 284 (2013) 319–323.
[8] Z. Wang, Y. Su, Q. Li, Y. Liu, Z. She, F. Chen, L. Li, X. Zhang, P. Zhang, Researching a highly anti-corrosion superhydrophobic film fabricated on AZ91D magnesium alloy and its anti-bacteria adhesion effect, Mater. Charact. 99 (2015) 200–209.
[9] Q. Ma, W. Wang, G. Dong, Facile fabrication of biomimetic liquid-infused slippery surface on carbon steel and its self-cleaning, anti-corrosion, anti-frosting and tribological properties, Colloids Surf. A Physicochem. Eng. Asp. 577 (2019) 17–26.
[10] T.-S. Wong, S.H. Kang, S.K.Y. Tang, E.J. Smythe, B.D. Hatton, A. Grinthal, J. Aizenberg, Bioinspired self-repairing slippery surfaces with pressure-stable omniphobicity, Nature 477 (2011) 443.
[11] B. Bhushan, Y.C. Jung, Micro-and nanoscale characterization of hydrophobic and hydrophilic leaf surfaces, Nanotechnology 17 (2006) 2758.
[12] N.E. Zander, J.A. Orlicki, A.S. Karikari, T.E. Long, A.M. Rawlett, Super-hydrophobic surfaces via micrometer-scale templated pillars, Chem. Mater. 19 (2007) 6145–6149.
[13] L. Feng, S. Li, Y. Li, H. Li, L. Zhang, J. Zhai, Y. Song, B. Liu, L. Jiang, D. Zhu, Superhydrophobic surfaces: from natural to artificial, Adv. Mater. 14 (2002) 1857–1860.
[14] B.N. Sahoo, B. Kandasubramanian, Recent progress in fabrication and characterisation of hierarchical biomimetic superhydrophobic structures, RSC Adv. 4 (2014) 22053–22093.
[15] M. Ma, R.M. Hill, Superhydrophobic surfaces, Curr. Opin. Colloid Interface Sci. 11 (2006) 193–202.
[16] Z. Chen, L. Hao, A. Chen, Q. Song, C. Chen, A rapid one-step process for fabrication of superhydrophobic surface by electrodeposition method, Electrochim. Acta 59 (2012) 168–171.
[17] Z. Yang, X. Liu, Y. Tian, Fabrication of super-hydrophobic nickel film on copper substrate with improved corrosion inhibition by electrodeposition process, Colloids Surf. A Physicochem. Eng. Asp. 560 (2019) 205–212.
[18] J. Li, Y. Yang, F. Zha, Z. Lei, Facile fabrication of superhydrophobic ZnO surfaces from high to low water adhesion, Mater. Lett. 75 (2012) 71–73.
[19] S.S. Latthe, H. Imai, V. Ganesan, A.V. Rao, Superhydrophobic silica films by sol–gel co-precursor method, Appl. Surf. Sci. 256 (2009) 217–222.
[20] K. Teshima, H. Sugimura, Y. Inoue, O. Takai, A. Takano, Transparent ultra water-repellent poly (ethylene terephthalate) substrates fabricated by oxygen plasma

treatment and subsequent hydrophobic coating, Appl. Surf. Sci. 244 (2005) 619–622.
[21] B. Qian, Z. Shen, Fabrication of superhydrophobic surfaces by dislocation-selective chemical etching on aluminum, copper, and zinc substrates, Langmuir 21 (2005) 9007–9009.
[22] N. Zhao, F. Shi, Z. Wang, X. Zhang, Combining layer-by-layer assembly with electrodeposition of silver aggregates for fabricating superhydrophobic surfaces, Langmuir 21 (2005) 4713–4716.
[23] J.A. Syed, S. Tang, X. Meng, Super-hydrophobic multilayer coatings with layer number tuned swapping in surface wettability and redox catalytic anti-corrosion application, Sci. Rep. 7 (2017) 4403.
[24] T. Hang, A. Hu, H. Ling, M. Li, D. Mao, Super-hydrophobic nickel films with micro-nano hierarchical structure prepared by electrodeposition, Appl. Surf. Sci. 256 (2010) 2400–2404.
[25] S. Khorsand, K. Raeissi, F. Ashrafizadeh, Corrosion resistance and long-term durability of super-hydrophobic nickel film prepared by electrodeposition process, Appl. Surf. Sci. 305 (2014) 498–505.
[26] J. Tam, G. Palumbo, U. Erb, Recent advances in superhydrophobic electrodeposits, Materials 9 (2016) 151.
[27] H. Liu, L. Feng, J. Zhai, L. Jiang, D. Zhu, Reversible wettability of a chemical vapor deposition prepared ZnO film between superhydrophobicity and superhydrophilicity, Langmuir 20 (2004) 5659–5661.
[28] Z. Yang, X. Liu, Y. Tian, Hybrid laser ablation and chemical modification for fast fabrication of bio-inspired super-hydrophobic surface with excellent self-cleaning, stability and corrosion resistance, Journal of Bionic Engineering 16 (2019) 13–26.
[29] W. Zhang, Z. Yu, Z. Chen, M. Li, Preparation of super-hydrophobic Cu/Ni coating with micro-nano hierarchical structure, Mater. Lett. 67 (2012) 327–330.
[30] B. Pijáková, M. Klíma, M. Alberti, V. Buršíková, Facile electrodeposition of superhydrophobic and oil-repellent thick layers on steel substrate, Mater. Lett. 184 (2016) 243–247.
[31] A. Haghdoost, R. Pitchumani, Fabricating superhydrophobic surfaces via a two-step electrodeposition technique, Langmuir 30 (2014) 4183–4191.
[32] G. He, S. Lu, W. Xu, S. Szunerits, R. Boukherroub, H. Zhang, Controllable growth of durable superhydrophobic coatings on a copper substrate via electrodeposition, Phys. Chem. Chem. Phys. 17 (2015) 10871–10880.
[33] G. Zhao, J. Li, Y. Huang, L. Yang, Y. Ye, F.C. Walsh, J. Chen, S. Wang, Robust Ni/WC superhydrophobic surfaces by electrodeposition, RSC Adv. 7 (2017) 44896–44903.
[34] S. Jiang, Z. Guo, G. Liu, G.K. Gyimah, X. Li, H. Dong, A rapid one-step process for fabrication of biomimetic superhydrophobic surfaces by pulse electrodeposition, Materials (Basel, Switzerland) 10 (2017) 1229.
[35] S. Imanian Ghazanlou, A.H.S. Farhood, S. Ahmadiyeh, E. Ziyaei, A. Rasooli, S. Hosseinpour, Characterization of pulse and direct current methods for electrodeposition of Ni-Co composite coatings reinforced with nano and Micro ZnO particles, Metall. Mater. Trans. A 50 (2019) 1922–1935.
[36] Z.H. Gretić, E.K. Mioč, V. Čadež, S. Šegota, H. Otmačić Ćurković, S. Hosseinpour, The influence of thickness of stearic acid self-assembled film on its protective properties, J. Electrochem. Soc. 163 (2016) C937–C944.
[37] Z. Hajdari, H.O. Ćurković, V. Čadež, S. Šegota, Corrosion protection of cupronickel alloy by self-assembled films of fatty acids, J. Electrochem. Soc. 163 (2016) C145–C155.
[38] Z. Chen, F. Tian, A. Hu, M. Li, A facile process for preparing superhydrophobic nickel films with stearic acid, Surf. Coat. Technol. 231 (2013) 88–92.
[39] A.B. Gurav, S.S. Latthe, R.S. Vhatkar, J.-G. Lee, D.-Y. Kim, J.-J. Park, S.S. Yoon, Superhydrophobic surface decorated with vertical ZnO nanorods modified by stearic acid, Ceram. Int. 40 (2014) 7151–7160.
[40] N. Saleema, M. Farzaneh, Thermal effect on superhydrophobic performance of stearic acid modified ZnO nanotowers, Appl. Surf. Sci. 254 (2008) 2690–2695.
[41] J. Zhang, Z. Liu, J. Liu, E. Lei, Z. Liu, Effects of seed layers on controlling of the morphology of ZnO nanostructures and superhydrophobicity of ZnO nanostructure/stearic acid composite films, Mater. Chem. Phys. 183 (2016) 306–314.
[42] J. Tan, J. Hao, Z. An, C. Liu, Simple fabrication of superhydrophobic nickel surface on steel substrate via electrodeposition, Int. J. Electrochem. Sci. 12 (2017) 40–49.
[43] E. Naseri, M. Hajisafari, A. Kosari, M. Talari, S. Hosseinpour, A. Davoodi, Inhibitive effect of Clopidogrel as a green corrosion inhibitor for mild steel; statistical modeling and quantum Monte Carlo simulation studies, J. Mol. Liq. 269 (2018) 193–202.
[44] E. Khamis, F. Bellucci, R.M. Latanision, E.S.H. El-Ashry, Acid corrosion inhibition of nickel by 2-(triphenosphoranylidene) succinic anhydride, CORROSION 47 (1991) 677–686.
[45] M. Talari, S. Mozafari Nezhad, S.J. Alavi, M. Mohtashamipour, A. Davoodi, S. Hosseinpour, Experimental and computational chemistry studies of two imidazole-based compounds as corrosion inhibitors for mild steel in HCl solution, J. Mol. Liq. 286 (2019) 110915.
[46] N. Hassan, R. Holze, A comparative electrochemical study of electrosorbed 2- and 4-mercaptopyridines and their application as corrosion inhibitors at C60 steel, J. Chem. Sci. 121 (2009) 693.
[47] A. Kosari, M.H. Moayed, A. Davoodi, R. Parvizi, M. Momeni, H. Eshghi, H. Moradi, Electrochemical and quantum chemical assessment of two organic compounds from pyridine derivatives as corrosion inhibitors for mild steel in HCl solution under stagnant condition and hydrodynamic flow, Corros. Sci. 78 (2014) 138–150.
[48] S. Khorsand, K. Raeissi, F. Ashrafizadeh, M.A. Arenas, Super-hydrophobic nickel–cobalt alloy coating with micro-nano flower-like structure, Chem. Eng. J. 273 (2015) 638–646.
[49] E. Rahimi, A. Davoodi, A.R.K. Rashid, Characterization of screw dislocation-driven growth in nickel micro-nanostructure electrodeposition process by AFM, Mater. Lett. 210 (2018) 341–344.
[50] E. Rahimi, A. Rafsanjani-Abbasi, A. Imani, A.R. Kiani Rashid, S. Hosseinpour, A. Davoodi, Synergistic effect of a crystal modifier and screw dislocation step defects on the formation mechanism of nickel micro-nanocone, Mater. Lett. 245 (2019) 68–72.
[51] F. Meng, S.A. Morin, A. Forticaux, S. Jin, Screw dislocation driven growth of nanomaterials, Acc. Chem. Res. 46 (2013) 1616–1626.
[52] J.M. Lee, K.K. Jung, J.S. Ko, Formation of nickel microcones by using an electrodeposition solution containing H3BO3, Curr. Appl. Phys. 16 (2016) 261–266.
[53] S. Hosseinpour, J. Hedberg, S. Baldelli, C. Leygraf, M. Johnson, Initial oxidation of alkanethiol-covered copper studied by vibrational sum frequency spectroscopy, J. Phys. Chem. C 115 (2011) 23871–23879.
[54] J.W. Nibler, Infrared absorption spectroscopy. Second edition (Nakanishi, Koji), J. Chem. Educ. 55 (1978) A316.
[55] P. Wang, D. Zhang, R. Qiu, B. Hou, Super-hydrophobic film prepared on zinc as corrosion barrier, Corros. Sci. 53 (2011) 2080–2086.
[56] R.N. Wenzel, Resistance of solid surfaces to wetting by water, Industrial & Engineering Chemistry 28 (1936) 988–994.
[57] M. Guo, P. Diao, S. Cai, Highly hydrophilic and superhydrophobic ZnO nanorod array films, Thin Solid Films 515 (2007) 7162–7166.
[58] A.B.D. Cassie, S. Baxter, Wettability of porous surfaces, Trans. Faraday Soc. 40 (1944) 546–551.
[59] E. McCafferty, Introduction to Corrosion Science, Springer Science & Business Media, 2010.